

Laser Raman Micro-spectroscopy as an Effective Non-Destructive Method of Detection and Identification of various sp^2 Carbon Modifications in Industry and in Nature**

Sergey S. Bukalov*, Larissa A. Leites, Rinat R. Aysin

*Russian Academy of Sciences, Scientific and Technical Center on Raman Spectroscopy,
A.N. Nesmeyanov Institute of Organoelement Compounds, Vavilova str. 28, Moscow 119991, Russia*

*Corresponding author: E-mail: buklei@ineos.ac.ru; Tel: +7(499)135-92-62

Received: 04 September 2018, Revised: 06 December 2018 and Accepted: 08 January 2019

DOI: 10.5185/amlett.2019.2268
www.vbripress.com/aml

**Dedicated to the 90th anniversary of the Raman effect (modified-frequency scattering of monochromatic light) discovered simultaneously and independently by Raman (India) and academicians Mandel'stam and Landsberg (USSR).

Abstract

Raman micro-spectroscopy is recommended as an effective non-destructive method of detection and identification of various sp^2 carbon modifications, each being characterized by its own specific set of spectral band parameters (frequencies, intensities, half-widths and contours). The results of the authors obtained for numerous industrial sp^2 carbon samples (highly ordered and disordered graphites, turbostratic graphite, glassy carbons, carbon fibers, amorphous sp^2 carbon, nanotubes) as well as for natural species (terrestrial natural graphites and shungites, Lunar soil, meteoritic matter) are summarized, analyzed and compared. Literature data are also considered and discussed. The results show that the man-made advanced materials contain the same sp^2 carbon modifications as have been found in Nature (on Earth, Moon and in cosmic space). Copyright © VBRI Press.

Keywords: Raman micro-spectroscopy, sp^2 carbon modifications.

Introduction

Raman spectroscopy (inelastic, modified-frequency scattering of monochromatic light) was discovered independently and simultaneously by Raman (India) and acad. Mandel'stam and Landsberg (USSR) 90 years ago [1, 2]. A recent progress in technology has led to emergence of high-sensitive laser Raman spectrometers equipped with microscopes and TV cameras and with cooled CCD detectors that allow one to obtain micro-Raman spectra with spatial resolution of $\sim 1 \mu\text{m}$. This method on its modern level turned out to be indispensable in detection and identification of various sp^2 carbon modifications even in heterogeneous materials where carbon is present in micro-quantities. Computer search with keywords “ sp^2 carbon” and “Raman”, starting with 2007 on, has resulted in ~ 1000 references.

It is well-known that sp^2 carbon materials (CMs) in their different forms (highly oriented graphite, disordered graphites, glassy carbon, carbon fibers, carbon black, carbon nanotubes etc.) are widely used in modern high-tech industry, in various branches of engineering and electrotechnics, chemistry, metallurgy, atomic and space industries [3] and thus are of great

current interest. Therefore, it is very important to have at one's disposal an analytical non-destructive tool of CM detection, which is able to determine CM structural characteristics, degree of ordering and homogeneity. This is possible because each sp^2 carbon modification exhibits a specific Raman spectrum with its own band parameters. In this paper we will not delve into theoretical grounds of this field based on the solid-state theory, their present status is expanded in numerous publications (see, e.g, a comprehensive review [4]).

Our aim is to present to a reader who is not a specialist in Raman spectroscopy a phenomenological, empirical approach to characterize CMs in monitoring and control of manufacturing processes. Knowledge of the Raman spectra of various CMs and distinctions between them would help in CM identification in various composites as well as in natural matters.

Raman spectra of many CMs have been already described and discussed in numerous papers and monographs [4-20]. Our study differs from others in that we have measured to a high accuracy not only band frequencies, but also intensities and their ratios, half-widths (full width at half-maximum - FWHM), and contours. We were also among the first to carry out sample micro-mapping. This paper is a review of the

results of our systematical long-term studies of the Raman spectra of various sp^2 CMs of different origin, industrially produced and natural. Our representation begins with the factory-made samples whose structure was reliably established by various physicochemical methods; the thorough analysis of their Raman spectra has helped us in identifying natural substances.

The Raman spectra of sp^2 CMs. Graphene and industrial graphites

The vibrational spectra of sp^2 CMs are very simple and can be divided into the first (1000-1700 cm^{-1}) and second order (2400-3200 cm^{-1}) regions. The simplest, “prototype” Raman spectrum is exhibited by the mono-layer graphene, the building block of many sp^2 CMs. Its Raman spectrum with 5145 nm excitation was first published by Ferrari *et al.* [21]. We have recorded this spectrum from a sample prepared by mechanical exfoliation of graphite and mounted on a Si substrate, it is given in Fig. 1a (hereinafter the spectra presented were measured at 632.8 nm excitation). In accord with the data [21,22], the spectrum contains only two features. These are the first-order symmetry-allowed band at $\sim 1582\text{ cm}^{-1}$ (labeled G for “graphene, graphite”) that corresponds to a degenerate E_{2g} vibrational mode which represents tangential displacement of the carbon atoms in the basic plane (Fig. 2a) and also a second-order, very intense symmetric line at $\sim 2650\text{ cm}^{-1}$. In some papers the latter is designated as G' , but we prefer a more correct symbol 2D (see below). Both graphene lines obtained are extremely narrow, FWHM values are 10 and 20 cm^{-1} for G and D lines, respectively. The spectrum of monocrystalline hexagonal graphite first published in 1970 [23] also exhibits the G line at $\sim 1582\text{ cm}^{-1}$ with FWHM=12.5 cm^{-1} (Fig. 1b) but differs from that of graphene in the second-order region where it shows a less-intense feature of a complicated contour. In the Raman spectra of less ordered graphites, new first-order lines appear (Fig. 1c). The so-called D-line (labeled for “disorder, defects”) is observed in the region $\sim 1340\text{ cm}^{-1}$, its exact frequency depends on the wavelength of the exciting line. With 632.8 nm excitation, its frequency lies in the region 1325-1340 cm^{-1} . The origin of the D line has been analyzed in many papers (see review [4] and references therein). It is assigned to the A_{1g} “breathing” mode of the hexagons (Fig. 2b) that is forbidden in Raman for “perfect” graphite and activates due to selection rules relax in an imperfect crystal lattice.

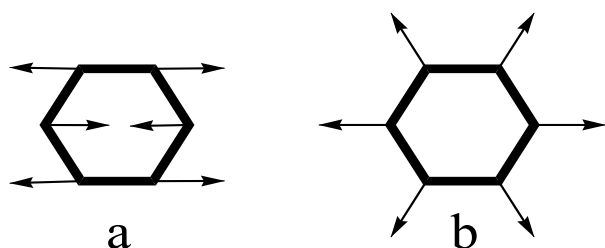


Fig. 2. Eigenvectors of the G (a) and D (b) normal modes.

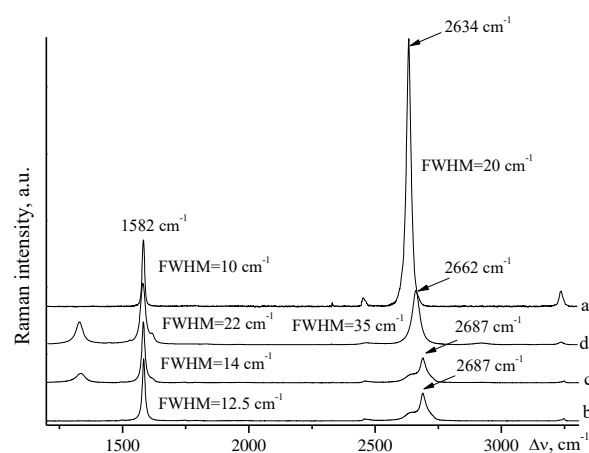


Fig. 1. Typical Raman spectra of a mono-layer graphene (a), highly oriented hexagonal graphite (b), slightly disordered hexagonal graphite (c) and turbostratic graphite (d).

As the frequency of the second-order band at $\sim 2700\text{ cm}^{-1}$ is twice that of the D line, it is evident that this band belongs to the overtone of D, and thus the designation 2D is well-grounded.

Along with the D line, in the spectra of disordered graphites a second disorder-induced weak D' line appears at 1600-1620 cm^{-1} as a shoulder of the G line (Figs. 1, 3).

We have measured the Raman spectra of more than 1500 samples of various factory-made graphites. Typical evolution of the Raman spectrum of graphite with its disordering is given in Fig. 3. It is evident that disordering leads to broadening and shifting of the Raman features. It is seen that the intensity and half-width of the D line vary depending on the sample origin. At appearance and growth of the D line, the frequency of the G line varies within the limits 1570-1585 cm^{-1} while its half-width increases from 13 to 25 cm^{-1} . It is also notable that in all the graphite spectra the intensity of the D line is always less than that of the G line (the ratio $I_D/I_G < 1$). This ratio was used by Tuinstra and König [23] for characterization of the graphite particle size in the basic plane L_a with use of an empirical formulation where C is an empirical constant depending on the excitation wavelength λ :

$$L_a = C(\lambda) (I_D/I_G)^{-1} \quad (1)$$

This “König’s formulae” was modified and widely used by many authors. However its applicability was doubted [24-27] on the basis of strict comparison of the Raman and XRD data for one and the same graphite samples. The main argument [24, 25] is that physical nature of XRD and Raman experiments differs significantly. In particular, the laser beam penetrates into a black carbonaceous material at a depth of $\sim 15\mu m$ [28] whereas XRD provides information volume-averaged over several cubic millimeters. Besides, XRD better “sees” the bigger crystallites, whereas formulae (1) underestimates L_a , being more sensitive to small

crystallites. These only arguments make a direct correlation of XRD and Raman data incorrect. However, the relation I_D/I_G ratio vs crystallite size is still widely used even nowadays. In its modified and upgraded version it is applied to nano-crystalline species in numerous publications [4, 7, 8, 22, 15, 28-32] to calculate the size of planar graphitic domains and the interdefect distance.

The second-order Raman spectrum of graphites depends on the origin of the sample. Highly crystalline hexagonal graphite samples exhibit the 2D band of a complicated contour and of medium intensity in the region 2600-2800 cm^{-1} as well as very weak features at 2460 and 3250 cm^{-1} (see **Figs. 1b, 3**). An increase in the D line intensity leads to a slight change in the shape of the 2D band (**Fig. 3**).

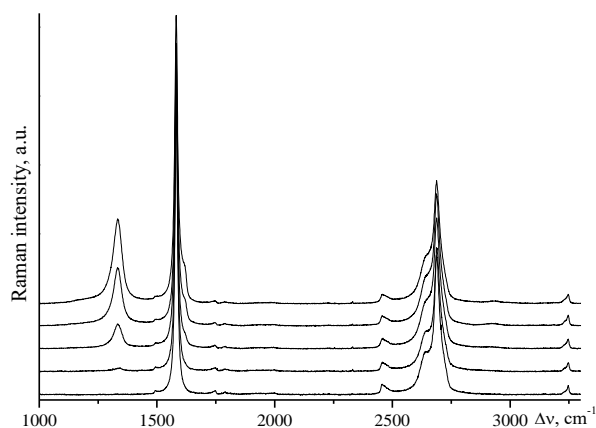


Fig. 3. Evolution of the Raman spectrum of graphite with its gradual disordering.

Statistical treatment of the bulk data obtained has allowed us to set forward the following criterium [24]: from the viewpoint of Raman spectroscopy, a carbon material can be classified as hexagonal graphite if its Raman spectrum exhibits the G line at 1570-1585 cm^{-1} with a half-width 12-25 cm^{-1} along with the D line at 1325-1340 cm^{-1} (with 632.8 nm excitation) of variable intensity and half-width $\geq 30 \text{ cm}^{-1}$, whereas the intensity ratio $I_D/I_G < 1$.

As was reported [22], transformation of monocrystalline graphite into nano-crystalline one (with a decrease in averaged crystallite size up to ~20 nm) is followed by an increase in the I_D/I_G ratio to values >1 with a simultaneous upshift of the G line to ~1600 cm^{-1} .

Another specific form of graphite is the so-called “turbostratic” or “expanded” graphite which lacks three-dimensional (3D) order because there is no regular orientation of the graphene layers about the hexagonal axis. Its interlayer distance is increased to 3.44 Å, as compared to that of the perfect 3D graphite 3.354 Å. The Raman spectrum of a turbostratic graphite sample presented in **Fig. 1d** exhibits the same I_D/I_G ratio <1 , just as that for graphites, but it differs from the spectrum of customary graphite by its second-order region where a narrow symmetric 2D line at ~2665 cm^{-1}

with a half-width 35 cm^{-1} is observed. It is pertinent to note here that a single symmetric 2D band is specific to all the sp^2 carbonaceous materials that have no three-dimensional order (mono-layer graphene, turbostratic graphite, glassy carbon, single-wall nanotubes, *etc.*, see below).

Glassy carbon

Glassy carbon (GC) is a sp^2 CM produced by pyrolysis of suitable thermoreactive organic polymers. Owing to its unique physicochemical properties, such as isotropy, chemical inertness, high mechanical strength, low density due to the presence of high proportion of closed pores, impermeability to gases and liquids, extreme resistance to chemical attack, electrical conductivity, heat conduction, biocompatibility, this material is widely used in modern high technologies [3, 33, 34]. GC belongs to the so-called “non-graphitizable” CMs which do not transform to graphite even at temperatures of up to 3000 °C [33, 35]. Several models were proposed for GC structure based on the X-ray and neutron diffraction results as well as Raman spectroscopy, TEM, SEM, and AFM data and on model calculations [33-43].

We have followed structural changes in the samples of a typical non-graphitizable CM (fabricated at the pilot factory of the State Research Institute of Graphite, Moscow) produced by carbonization of phenol-formaldehyde resin and heat-treated in a step-wise manner under an inert atmosphere in the interval from 1020 °C to 2700 °C (the samples are labeled according to the annealing temperature as GC1020 etc). To characterize the samples, Raman spectroscopy as well as elemental analysis and XRD data were used [44]. All these measurements need no preliminary sample preparation.

Raman spectra of GC of various origins have been already published and interpreted [14, 19, 23, 24, 45, 46]. Our results presenting evolution of the Raman spectra vs annealing temperature are given in **Fig. 4**, the band parameters are characterized in **Table 1**. The overall spectral patterns agree well with the literature data.

At initial stage of the pyrolysis (up to ~1050 °C) primary carbonization and polymerization of the organic substance take place with formation of randomly oriented graphene layers, however, containing an appreciable fraction of heteroatoms. Indeed, our elemental analysis data show that the sample GC1020 contains only 75% of carbon. The Raman spectrum of GC1020 (the lowest spectrum in **Fig. 4**) exhibits in the region 1000-2000 cm^{-1} very broad D and G bands. In its second-order Raman spectrum (2600-3200 cm^{-1}) very broad weak features are observed. All this is typical of highly disordered sp^2 CMs [see below, part 3]. The D and G bands broadening and lowered carbon content evidence that the sample marked GC1020 is in essence not a real glassy carbon.

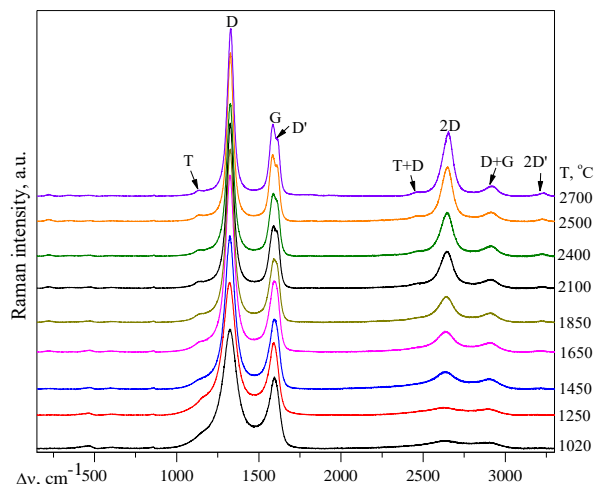


Fig. 4. Raman spectra of the GC samples annealed at different temperatures and the band assignment.

It is only in the GC1650 sample that carbon content reaches the value of 99.5 % while its Raman spectrum exhibits noticeable changes. At 1650°C and higher temperatures, the D and 2D bands shift slightly and gradually narrow (Table 1, Figs. 4, 5). The G line becomes more and more asymmetric, and at temperatures 1850° C and higher, new weak Raman peaks at 1620 cm⁻¹ (D') and ~1150 cm⁻¹ (T) show up. The latter feature was reported [47] for curved graphite whiskers. Thus, the first-order Raman spectrum of high-temperature GC differs from those of graphite in the widths of the D and G lines, in their intensity ratio $I_D/I_G > 1$ and in the presence of the T line. The second-order spectrum of high-temperature GC also differs significantly from that of graphite. An increase in the heat-treatment temperature leads to a gradual formation of an intense symmetric 2D band at ~2650 cm⁻¹. Such frequency and intensity values of this band and its symmetrical shape point to the absence of strict periodicity along the *c* axis. At annealing temperatures 1650°C and higher, the emergence of very weak bands in the low-frequency region of the Raman spectra (200-500 cm⁻¹) is also of note (Fig. 6). Analogous bands were observed for carbon tubular cones, whiskers, polyhedral crystals and nano-onions [47, 48], the authors associated them with graphene sheet curvature. For the latter CMs, a high Raman intensity and symmetrical shape of the 2D overtone were also observed, as in the spectrum of the GC2700 sample.

Table 1. Frequencies and half-widths (FWHM, cm⁻¹) of the D and 2D bands and I_D/I_G intensity ratios in the Raman spectra of glassy carbon samples.

Heat treatment temperature °C	D line frequency (FWHM), cm ⁻¹	I_D/I_G	2D line frequency (FWHM), cm ⁻¹
1020	1324.5 (107)	2.7	2637 (233)
1250	1326.5 (92)	2.7	2638 (213)
1450	1326.5 (69)	2.7	2639 (148)
1650	1328 (59)	2.7	2643 (113)
1850	1328 (53)	2.6	2645 (102)
2150	1328 (48)	2.2	2647 (88)
2450	1329 (42)	1.8	2649 (72)
2700	1329 (40)	1.6	2650 (67)

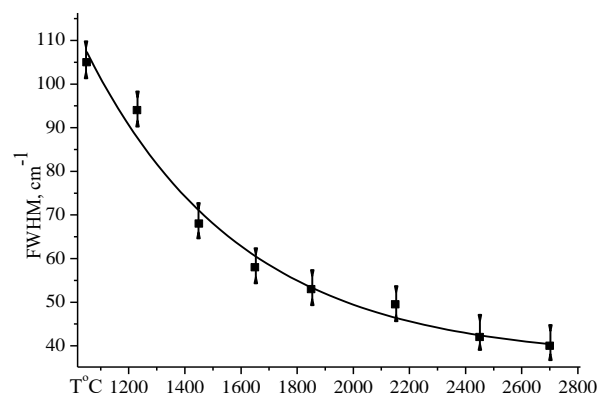


Fig. 5. Dependence of the D line half-width in the spectra of GC on the heat treatment temperature.

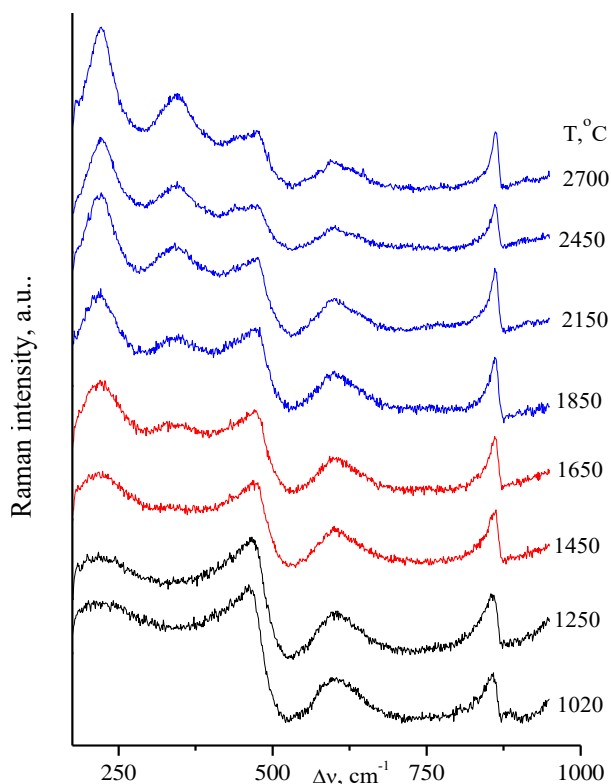


Fig. 6. Low-frequency Raman region of the GC spectra obtained.

Noticeable changes in the spectra of the GC samples heated at elevated temperatures, that is, band narrowing and a decrease in the value of I_D/I_G ratio along with the XRD results [44] bear evidence to an increase in two-dimensional order, that is, to a partial ordering of aromatic nano-clusters, increasing in size in the *ab* plane (two-dimensional “quasi-crystallization”). Gradual formation of new weak features in the Raman spectra (low-frequency ones and the T line) suggests appearance of curved carbon layers. However, the general structural motif, that is poorly ordered turbostratic graphitic nano-particles, is still preserved herewith. These facts speak well for applicability to the high-temperature GC samples of the structural model suggested by Harris [38, 39] which is based on “fullerene-related fragments” (sp² carbon sheets with high curvature including closed voids).

The results of the glassy carbons study allowed us to determine the structure of a product formed from turbostratic graphite after neutron irradiation (**Fig. 7**).

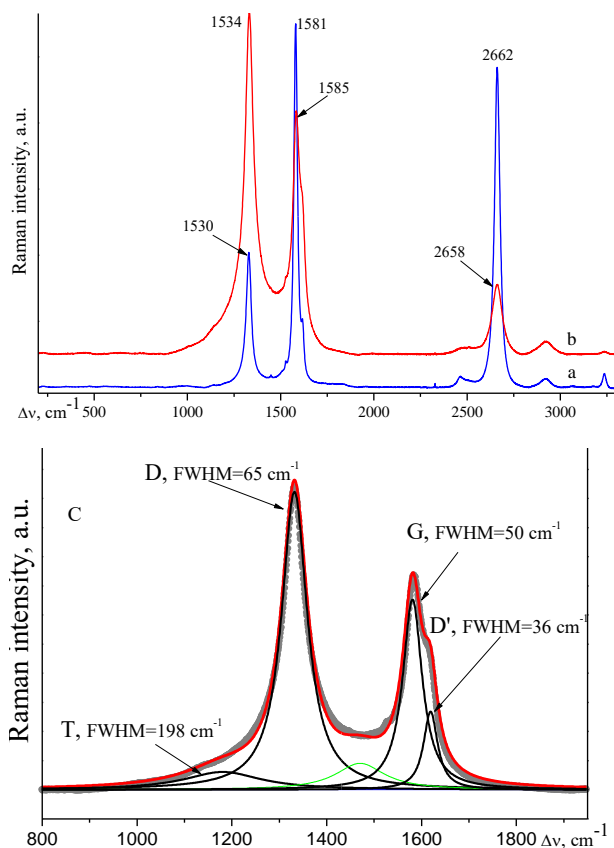


Fig. 7. The Raman spectrum of turbostratic graphite (a) and the product of its neutron irradiation (b), (c) - curve-fitting analysis of (b).

It is seen that in the spectral pattern of the irradiated sample alters significantly, the intensity of the D and 2D bands has increased noticeably and the I_D/I_G ratio becomes >1 . Curve-fitting analysis of the spectral region $900\text{-}1600\text{ cm}^{-1}$ (**Fig. 7c**) highlights the T band that points to the presence of curved elements. It is evident that the structure of the irradiated substance reminds that of GC.

Highly disordered sp^2 CM

This modification is designated by Robertson and Ferrari as a-C (sp^2 amorphous carbon [13, 14]). This material is characterized by a complete loss of periodicity. Here belong soot and carbon black. Soot is a product of an incomplete burning of carbon-containing species obtained under uncontrolled conditions and having no fixed properties. It contains not more than 90% of carbon [3]. **Fig. 8** presents the complicated Raman spectra of a car soot sample (a) and of a particle of Moscow smog (b). It is evident that these spectra contain not only the D and G bands of sp^2 carbon but also other features due to the presence of a significant amount of other species and an sp^3 carbon fraction [13, 14].

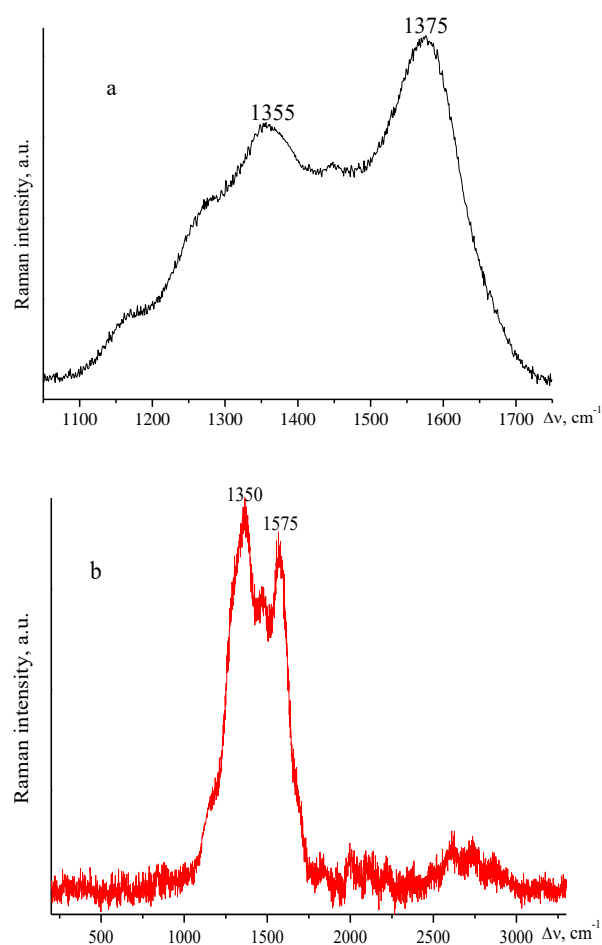


Fig. 8. Raman spectra of a car soot sample (a) and a particle of Moscow smog (b).

Technical carbon black has been used for many years in the rubber industry and produced on a large scale. According to the data of Refs. [16, 26, 39], it consists of globules of 10-50 nm size fused together to build up stable aggregates (up to 500 nm). These involve degraded graphite-like elements, interplane distance between the graphite-like layers being 0, 35-0, 365 nm.

The Raman spectrum of such a sample named "Vulcan" is given in **Fig. 9a**, the results of its curve-fitting analysis - in **Fig. 9b**. This spectrum agrees well with those reported in Ref. [16] and with the structural data. It is seen that carbon black is a more ordered material compared to soot. The presence of the T line at 1117 cm^{-1} is an evidence of curved elements. The positions of the D and G bands are shifted compared to graphite, their half-widths are extremely large (~ 210 and $\sim 130\text{ cm}^{-1}$, respectively) and the I_D/I_G ratio >1 . The spectrum **9a** is close to that presented for GC1020 in **Fig. 4**. This confirms that GC1020 sample corresponds to amorphous sp^2 carbon.

Thus, the Raman spectra of highly disordered sp^2 carbons are characterized by very broad D and G bands, the second-order region exhibiting weak broad features.

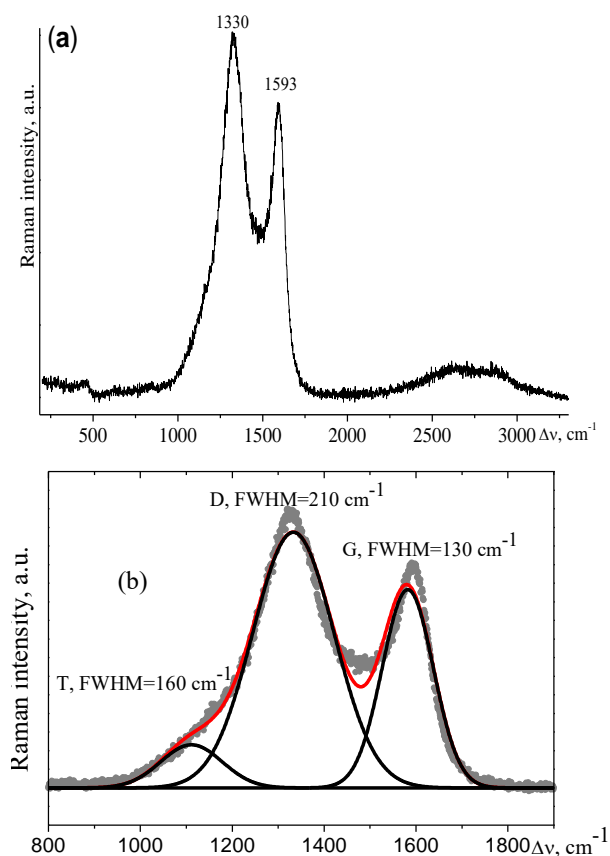


Fig. 9. Raman spectrum of the “Vulcan” carbon black sample (a) and the results of its curve-fitting analysis (b).

Carbon fibers

Carbon fibers (CF) manufactured based on polyacrylonitrilic (PAN) precursor are characterized by high mechanical strength, thermal and chemical stability, high elastic modulus and low density. These properties have determined extensive applications of CF as reinforcement materials for highly-effective polymer- and carbon-carbon composites [49-52]. Transformation of PAN structure into that of high-strength and/or high-modulus CF is accompanied by a change in chemical composition and proceeds in several stages. These are oxidative thermo stabilization at temperatures lower than 300 °C, carbonization (thermo-mechanical treatment at ~1600 °C) [50, 53], and a high-temperature treatment at ~2500 °C, leading to production of high-modulus fibers [54, 55].

Regularities of PAN transformation into thermostabilized fiber (TSF) were investigated by XRD, TEM, DSC, and TGA methods [30, 55-59]. Starting from the classical paper of Tuinstra and König [60], carbon fibers were also studied by Raman spectroscopy [30, 57, 61-67].

We present here the results of micro-Raman method that demonstrates the microstructure of small (~50 nm) regions of the material, and also the results of elemental analysis and XRD [68]. It is important to emphasize again that the XRD method, unlike Raman, provides volume-averaged information. The Raman

spectra were registered for both the fiber lateral surface (“skin”) and its cross-cut section (“core”). In the latter case the cut flake was settled vertically between two flat magnets and put under the microscope objective (magnification 50× and 100×) of the spectrometer. The authors of the papers [62, 63, 69] paid attention to the fact that the CF structure on its lateral surface differs from that in its center. To investigate this difference in detail, we carried out Raman measurements for the cross-cut CF section at various distances from the center. Before that, the Raman spectra of initial PAN filaments were obtained. They were registered for the filament skin as well as for its center (**Fig. 10**) and were found to coincide completely, thus demonstrating radial homogeneity of the sample. The most intense line at 2244 cm⁻¹ belongs to the νC≡N stretching mode.

In the Raman spectra of all the samples, taken in the process of CF manufacturing, the lines of PAN disappear gradually while the typical lines of the sp² carbon spectrum appeared and grew quickly. Transformation of the spectral pattern in the course of the whole process of CF fabrication is given in **Fig. 11a**, **Fig. 11b**, where **Fig. 11a** presents the spectra of the cut fiber center (averaged diameter of a mono-fiber is 7-8 μm) while **Fig. 11b** – those of lateral surfaces. Band assignment is given in **Fig. 11b**.

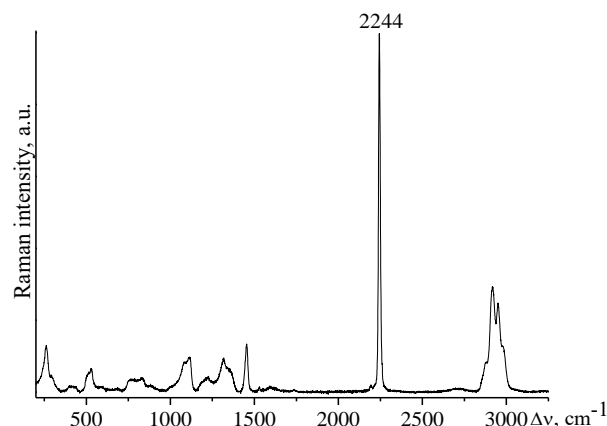


Fig. 10. The Raman spectrum of a PAN filament.

The frequencies and half-widths of the D and G bands are presented in **Table 2**.

Elemental analysis data (**Table 3**) show that it is only after heat treatment at ~2300°C in argon medium that the carbon content in the fiber reaches 95%; it increases to 97% only after further thermo-mechanical treatment at ~3000°C. This means that only the samples 4-6 are real “carbon fibers”.

Analysis of the data presented in **Fig. 11** and **Table 2** shows that the spectra of samples 2-4 registered for the skin and for the core coincide, indicating these samples homogeneity. Broadening of the D and G bands and the absence of a clear-cut second order spectrum point to a presence in these samples of disordered defective sp² clusters. After thermo-mechanical treatment of the fibers at ~3000°C, their spectra transform substantially.

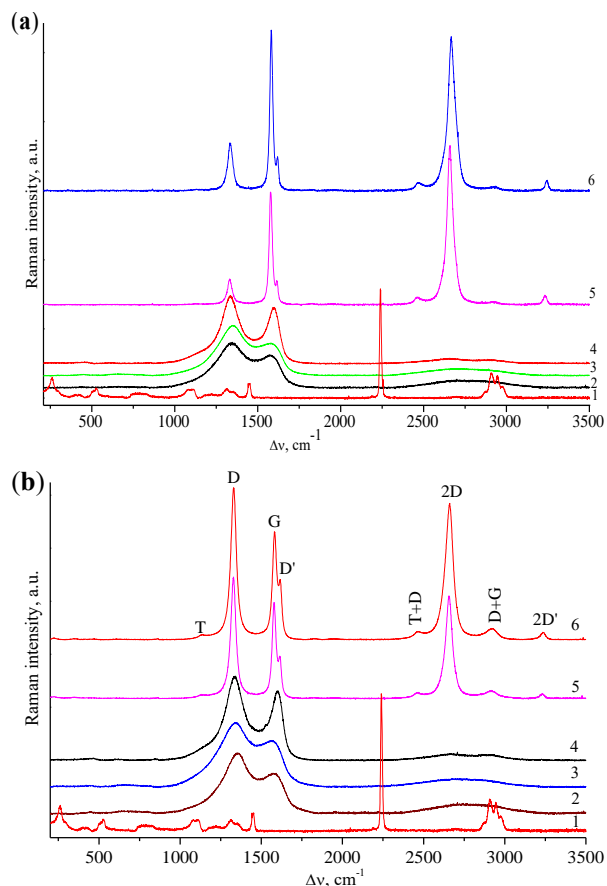


Fig. 11. Raman spectra of the CF samples registered for the fiber skin (a) and for its core (b). 1 – PAN filament, 2 – «underoxidized» filament, 3 – «oxidized» filament, 4 – CF (~2300°C), 5 – CF (~3000°C, E=410 GPa), 6 – CF (3000°C, E=496 GPa).

Table 2. Raman band characteristics in the spectra obtained for the samples taken in the process of CF manufacturing.

Carbon sample (number)	G band		D band		I _D /I _G	
	ν, cm ⁻¹	FWHM, cm ⁻¹	ν, cm ⁻¹	FWHM, cm ⁻¹		
“underoxidized” filament (2)	skin	1560-1565*	125-135	1350-1355*	165-175	~1.8
	core	1560-1565	125-135	1350-1355	165-175	
“oxidized” filament (3)	skin	1560-1565	125-135	1360-1365	165-175	~1.6
	core	1560-1565	125-135	1360-1365	165-175	
carbonized fiber (4) ~2300°C	skin	1590-1600	100	1335-1340	160	~1.4
	core	1590-1600	100	1335-1340	160	
carbonized fiber (5), ~3000°C, E = ~500 GPa	skin	1580-1585	20	~1330	25-30	0.2-0.3
	core	1580-1585	30	~1330	40-45	
carbonized fiber (6), ~3000°C, E = 410 GPa	skin	1580-1585	20	~1330	25-30	0.2-0.3
	core	1580-1585	30	~1330	40-45	
glassy carbon (Fig. 4)	1584	30-35	~1330	40	~2	
turbostratic graphite (Fig. 1d)]	1582	22	~1330	~30	~0.3	

*positions of the G and D lines were determined as a result of computer curve-fitting analysis of the overlapping contours.

Table 3. Elemental analysis data for the CF samples studied.

Sample number	% N	% C	% H
5	0.32	97.40	0.51
6	0.37	97.02	0.51
4	2.87	95.33	0.50
3	20.48	58.02	3.90
2	20.87	60.67	4.46

The second-order spectrum acquires now a distinct structure. High intensity and symmetrical shape of the 2D line in the spectra of CFs (~3000 °C) evidence the absence of three-dimensional ordering (by analogy with the spectra of turbostratic graphite (section 1), glassy carbon (section 2) and non-planar sp² materials [14, 47]). The G line narrowing leads to appearance of the D' line at ~1615 cm⁻¹. The spectra clearly demonstrate radial heterogeneity of these samples. Indeed, in the spectra of the fiber skin the I_D/I_G ratio is ~0.3, like that for graphites. However, in the spectra of the fiber core, the value of this ratio grows sharply up to 1.2-1.5 and a weak T band at ~1140 cm⁻¹ appears. These features juxtapose the spectra of the core with those of glassy carbons annealed at ~2700 °C. This is illustrated in Fig. 12.

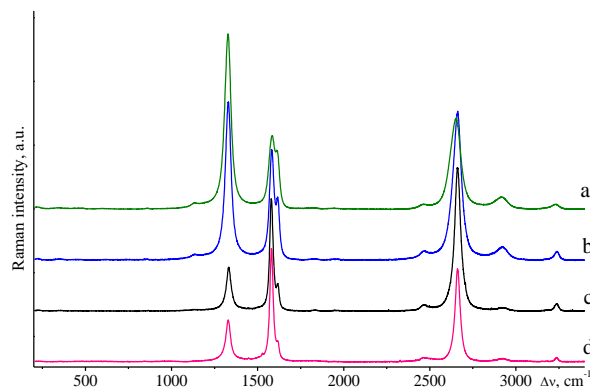


Fig. 12. Raman spectra of the carbon fiber (6) (~3000 °C in argon, E = 410 GPa). Blue curve (b) – fiber center, black curve (c) – lateral surface. For comparison the spectra are given of a glassy carbon annealed at ~2700 °C (green curve a) and of a sample of turbostratic graphite (red curve d).

Thus, our results confirm radial heterogeneity of carbon fibers disclosed previously but reject its treatment in terms of a model “rigid skin - soft core” proposed in Ref. [56]. Identity of the spectra of the fiber core and of the high-temperature glassy carbon points to closeness of their structures. Meanwhile, glassy carbon is not a soft material. As was said above, it is a hard isotropic non-graphitizable material, composed of disordered multi-layer curved nano-graphene fragments [38, 39].

For a more detailed study of radial heterogeneity of a mono-fiber, we have registered Raman spectra of the CF cross-cut section by a micro-mapping method with a step of ~0.2 μm, for each step the half-width of the D band and the I_D/I_G ratio were measured. The dependence of the D band half-width on the distance from the fiber surface to its center is given in Fig. 13.

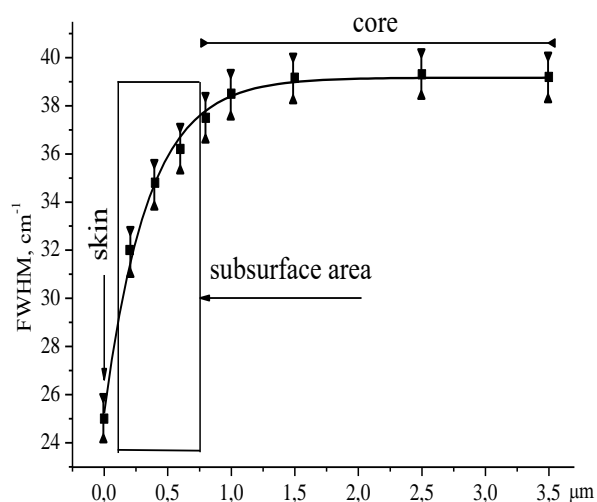


Fig. 13. The dependence of the D band half-width in the Raman spectra of the CF sample **6** ($\sim 3000^\circ$) on the distance from the fiber surface to its center.

It is seen that the radially heterogeneous substance of a mono-fiber cut can be approximately divided into three regions. These are the thin ($\sim 0.1 \mu\text{m}$ size) skin which is close in structure to turbostratic graphite, an intermediate boundary layer (up to $\sim 1 \mu\text{m}$ size), in whose spectrum the half-width of D line gradually increases from ~ 30 to $\sim 40 \text{ cm}^{-1}$ and I_D/I_G ratio rises sharply from ~ 0.3 to ~ 1.5 , and the core, where these parameters remain constant and close to those of high-temperature glassy carbon.

Carbon nanotubes

Single-wall carbon nanotubes (SWNT) were first synthesized systematically in 1993 and soon became a point of great interest due to their unique chemical, mechanical, thermal, optical, optoelectronic and electronic properties leading to a wide range of applications. SWNT are the most studied, both theoretically and experimentally [4, 5, 7, 8, 12, 70, 71]. The Raman spectra of SWNT stand in marked contrast to those of other sp^2 carbons by the presence of a low-frequency feature that corresponds to a totally-symmetric radial breathing mode (RBM) of a nanotube and is a real SWNT fingerprint. The frequency of the RBM was shown to linearly correlate with the reciprocal tube diameter d :

$$\nu \text{ (cm}^{-1}\text{)} = C/d+B, \quad (2)$$

where, C and B are variable constants depending on environmental effects [4]. The splitting of the G band in two components is also observed due to symmetry lowering and degeneracy lifting. The 2D band in these spectra is intense and symmetric. **Fig. 14** exemplifies this by presenting our results obtained for a SWNT bundle prepared by an electric arc method with use of a Ni/Y catalyst and purified to carbon content 95 % [72].

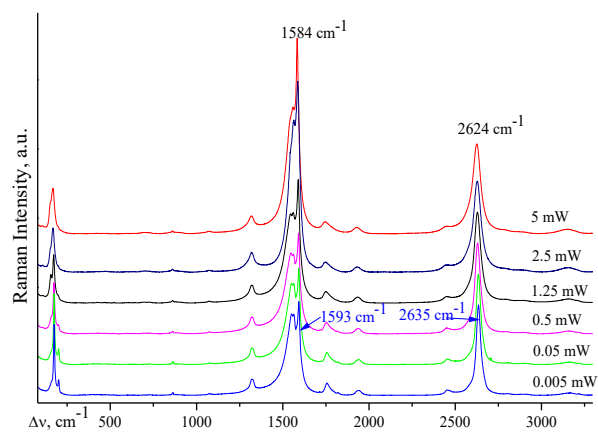


Fig. 14. Evolution of the Raman spectra of a SWNT bundle with an increase in the exciting line power

When working with SWNT Raman spectra, one should be very careful with the laser power because the spectrum is very sensitive to its magnitude [73]. We have also observed this effect, recording the spectra with variable exciting line power (from 0.005 to 5 mW). At low power values (0.05 mW and less) the spectrum remains constant. However, with an increase in the laser power above 0.05 mW, the spectrum alters significantly (**Fig. 14**). In particular, the frequency of the 2D line downshifts by $\sim 10 \text{ cm}^{-1}$ and its half-width increases from 33 to 65 cm^{-1} , the RBM region also alters noticeably. These changes could be a consequence of sample heating as well as of structural transformations. The authors [74] also advised to take special precautions in relation to laser power when obtaining Raman spectra of sp^2 carbons.

Conclusions based on the results of the Raman study of the man-made sp^2 carbon samples

Summing up the Raman results obtained for various industrially-produced sp^2 carbon samples, whose structure was experimentally defined by the armamentarium of physicochemical techniques, one can conclude that:

1. All these spectra include the main G and D first-order features, but they differ in their frequencies, intensities, shapes and half-widths, the latter values increasing with the degree of disorder.
2. The intensity ratio I_D/I_G is an important characteristic. Its value is less than unity for graphites (both hexagonal and turbostratic) and more than unity for nano-systems having no 3D order. This value allows one to qualitatively compare the crystallite size of sp^2 carbons ("larger or smaller") but not to quantitatively estimate L_a .
3. The second-order part of the spectrum is also significant. The band corresponding to the 2D overtone is weak and exhibits a complicated contour for graphites and amorphous carbons while it is intense and symmetric in the spectra of samples having no 3D order.

- Appearance of a weak T line in the region 1100-1200 cm^{-1} indicates curving of some graphene layers.
- Micro-Raman mapping permits one to conclude about homogeneity/heterogeneity of the sample. With this knowledge in mind, we can turn to investigation of natural sp^2 carbons, to elucidation their structure and degree of order.

Terrestrial sp^2 carbons

Natural graphites

We have studied many natural graphites of different origin (Ceylon, Vietnam, Dzhezkazgan, Botogol etc.). Their Raman spectra meet all the conditions [24] formulated above. The results of micro-mapping with spatial resolution 0.1 mm for a Ceylon graphite sample pictured in Fig. 15, which contains 99.9 % of carbon and is highly ordered according to the XRD data, are presented below.

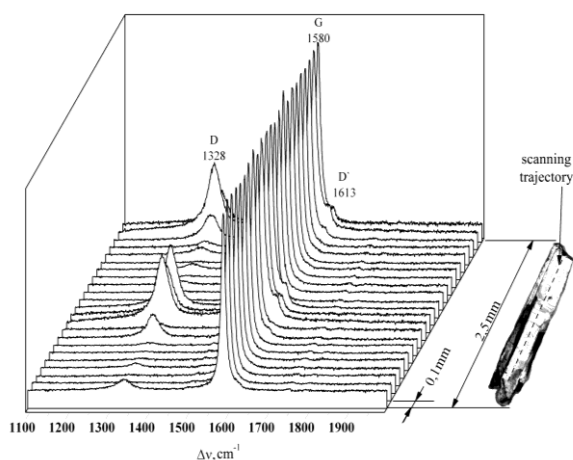


Fig. 15. The Raman spectra of a piece of Ceylon graphite shown, recorded with spatial resolution 0.1 mm

It is seen that only about a half of all the spectra obtained exhibit no D band which points to perfect 3D structure of the sample; in the rest spectra the D band is present, its intensity and the I_D/I_G ratio vary point-to-point. Taking into account the König's formulae (1), this indicates a dispersion in crystallite size values. Thus, the data obtained demonstrate that a sample of the Ceylon graphite which is known as highly-ordered is spatially "heterogeneous", nonuniform on a micro-level. Analogous results were obtained for other natural graphites [24]. Detailed examination of those spectra, selected from the set included in Fig. 15, which contain no D band, reveals unexpectedly that they differ in the second-order region (Fig. 16).

It is worthy of note that similar 2D patterns were reported in many papers (see, e.g., Refs. [22, 74]) as belonging to multi (bi-, three-, four-, five-) layer graphenes and were used to monitor the number of layers. One could hardly imagine that a piece of Ceylon graphite displayed in Fig. 15 contains such delicate species. Moreover, in the course of systematic precise

Raman measurements for a large set of Ceylon graphite samples, another unexpected result was obtained, namely, inclusions of a SWNT were detected, as it is evident from the spectrum presented in Fig. 17.

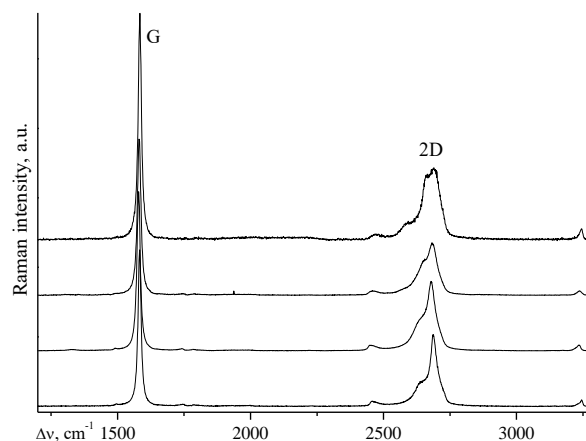


Fig. 16. The Raman spectra, containing no D band, recorded for some locations of the Ceylon graphite. Different 2D patterns are obvious.

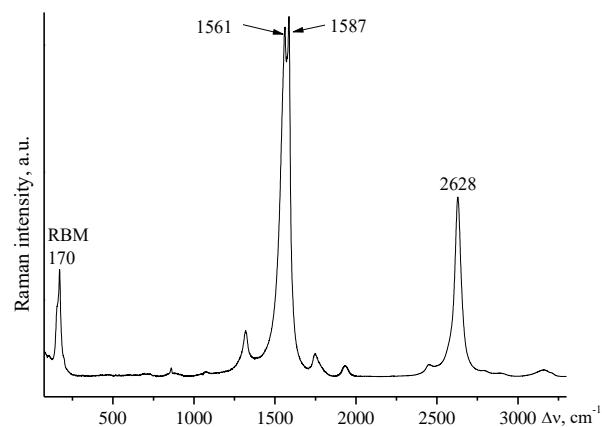


Fig. 17. The Raman spectrum of a SWNT inclusion obtained during the micro-mapping studies of a Ceylon graphite sample.

Thus, the sample of Ceylon graphite has appeared heterogeneous not only spatially but also structurally.

Karelian shungites

According to the literature data [75-79], carbonaceous component of Karelian shungites, carbon-rich rocks of Precambrian age, consists of globular sp^2 carbon nanoparticles with averaged size of 6-10 nm, agglomerated into complex multilayer compositions.

We have investigated several probes of Karelian shungites elected from Zazhoginskiy deposit. These were the samples from the original rock (the main matrix) having matted, opaque surface (labeled MAT) as well as discrete glittering surfaces (labeled GLITTER) of the so-called "tectonic slickensides". The latter are traditionally considered to be a consequence of a dynamic slip. Our aim was to reveal the difference between these two types of samples [80]. Determination of their elemental composition by the energy-dispersive X-ray analysis has shown that it varies to some extent

from one sample to another due to initial non-uniformity of the rock consistence as well as to secondary redistribution of the substances. The results of the measurements revealed an increase in carbon content in the slickenside films (compared to those in the main matrix), with a marked predominance of carbon over silicon. This is obviously a result of deformation in the displacement zone, leading to a sharp depletion of the substratum in silica and a corresponding enrichment in carbon.

We have investigated these samples by Raman spectroscopy in order to determine the local structure of their carbonaceous component. The spectra of the shungite surfaces MAT and GLITTER were obtained for two probes, ShV-1 and ShV-2, using micro-mapping method with spatial resolution 2 μm (Fig. 18).

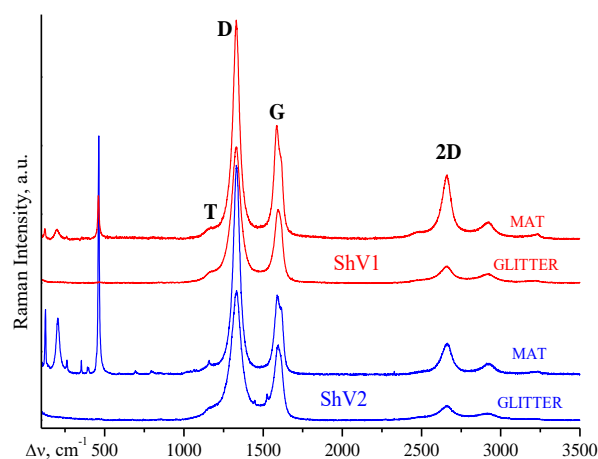


Fig. 18. Typical Raman spectra, obtained for the surfaces GLITTER and MAT of the shungite samples ShV-1 and ShV-2.

In the spectra of the GLITTER samples only the features characteristic of disordered sp^2 carbon modifications are observed, namely, the D, G and 2D bands. A weak T band is also present that characterizes the curvature of the graphene layers. The fact that in the GLITTER spectra only the bands of sp^2 carbon are observed but not those of accompanying minerals is explained by a small content of the latter. Besides, taking into account π -conjugated nature of the sp^2 carbon, its Raman spectrum should be strongly enhanced as compared to the spectra corresponding to minerals with their non-conjugated bonds. However, in the spectra of the MAT samples the lines of mineral components are clearly seen, which is in line with the increased content of the latter evidenced by elemental analysis data. The lines of mineral components are especially clearly seen in the spectrum of the sample SHV-1 recorded in the low-frequency region with an increased spectral gain (Fig. 19). The same Figure demonstrates different spectral patterns recorded for two different spots (a and b) of the MAT sample which agrees well with their different elemental content.

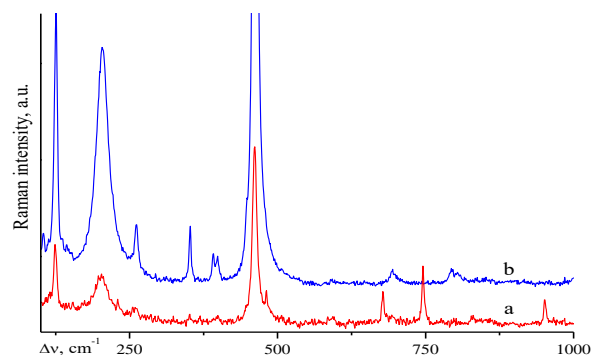


Fig. 19. The Raman spectra of the MAT sample SHV-1 in the low-frequency region, demonstrating the presence of minerals. The spectra are obtained for the two sample spots (a) and (b) which differ in elemental content.

In the Raman spectra of the GLITTER samples, the line D has a frequency of 1333 cm^{-1} and a half-width in the range of $65\text{--}67\text{ cm}^{-1}$. The D line in the spectra of the MAT samples is characterized by slightly different parameters, namely, the frequency at 1331 cm^{-1} and a half-width $55\text{--}57\text{ cm}^{-1}$ (the given values are averaged over a large data set). A noticeable widening of the D line in the spectra of the GLITTER slickensides, in comparison with that of the MAT, points to an increased disorder in the former sample. This could be associated with an increase in the degree of matrix damage in the course of deformation. The value of the intensity ratio I_D/I_G in all the spectra studied lies in the range of 2.0–2.3; this value is characteristic of sp^2 carbons disordered at nano-level.

In general, the Raman spectra obtained in this study for the carbonaceous components of natural shungites are very close to those of glassy carbon. Comparison of the parameters of the T, D, G and 2D bands in the Raman spectra of the shungite samples with similar characteristics in the spectra of the glassy carbons allows us to suggest that formation of the shungite sp^2 carbon took place in the temperature interval $1450\text{--}1650\text{ C}$. It could be assumed that this temperature was reached owing to the frictional heating.

Carbon in extra-terrestrial matter

We were fortunate enough to get at our disposal two extra-terrestrial materials, namely, the fragments of “Chelyabinsk” meteorite and the samples of Lunar soil.

Investigation of “Chelyabinsk” meteorite

It is well-known that in February of 2013 a meteorite has exploded over Russia near Chelyabinsk town with formation of many fragments, which have been investigated by several groups of Russian scientists. Preliminary geochemical analysis [81] has suggested that it was a stony meteorite with low iron content, of a chondrite type. The first data on mineral content and structure of some “Chelyabinsk” fragments have been published [82], based on optical reflection, SEM, X-ray diffraction, and TGA methods as well as chemical

analysis. Many minerals and many chemical elements were found herewith, the latter being mainly Si, Fe, Mg, etc., their total sum was reported as equal to 99.95% but no carbon was detected. A Raman study was also published [83] which identified several minerals but also not carbon (the spectra presented were limited up to 1300 cm^{-1} region), although the presence of a carbon-containing addition was assumed.

We have performed micro-Raman spectroscopy study of five meteorite fragments, the same as studied in Ref. [82]. The photographs of two of these, one fragment with the original black flowed surface and the second with a freshly cleaved grey surface, are presented in Fig. 20.



Fig. 20. Photographs of two fragments of “Chelyabinsk” meteorite studied: a fragment covered with a black flowed crust and a fragment with a freshly cleaved grey surface [84].

Both outer and freshly cleaved surfaces were investigated for all the samples available. More than 300 high-quality Raman spectra were registered which confirmed the presence in the meteorite of several minerals, detected previously [82, 83]. Besides that, we have found that the spectra obtained from some micro-sections of the freshly cleaved light-grey surfaces exhibit bands belonging to carbon species. The presence of carbon (0.11%) was also confirmed by the data of thorough elemental analysis [84].

In the nine of the spectra obtained a very narrow Raman line with a frequency at $1332\pm 1\text{ cm}^{-1}$ (FWHM = $3.5\pm 0.3\text{ cm}^{-1}$) was observed (see, e.g., Fig. 21), this unequivocally witnesses the presence of cubic diamond. The parameters of this line coincide with those diagnostic for perfect diamond crystals of terrestrial genesis [85-87].

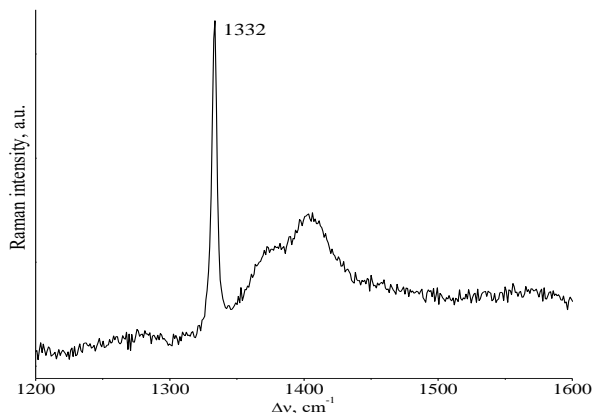


Fig. 21. Raman spectrum registered from a micro-zone inside the freshly cleaved meteorite surface, demonstrating presence of cubic diamond.

This result is not unexpected because diamonds had been often found in various meteorites, starting from 1888. The story of diamond and carbon identification in space was comprehensively expounded in Ref. [88].

For some other spots of the freshly cleaved meteorite surfaces, the Raman bands corresponding to the sp^2 carbon species (D at 1322 , G at 1598 and 2D at 2660 cm^{-1}) were detected along with mineral bands. This is exemplified in Fig. 22.

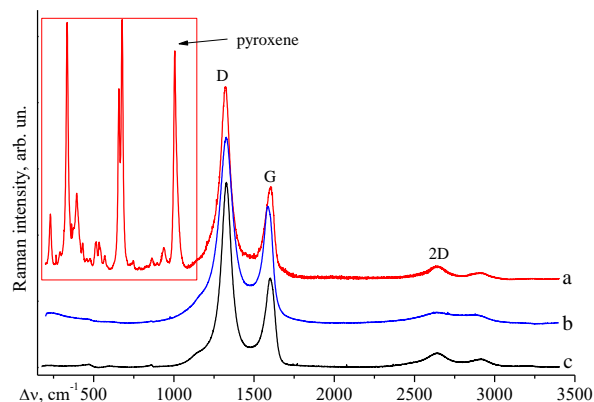


Fig. 22. Comparison of the Raman spectra of (a) a “Chelyabinsk” meteorite micro-segment inside the fresh cleavage, (b) a sample of Karelian shungite and (c) a sample of synthetic glassy carbon.

As seen from Fig. 22, the frequencies and half-widths of these bands as well as the value of I_D/I_G intensity ratio are close to those observed previously in the Raman spectra of Karelian shungites and synthetic glassy carbons (see above) which are in essence specific forms of nano-crystalline sp^2 carbon. Based on comparison with the data of Fig. 4, where a relation was found between the Raman spectra of glassy carbon samples and their heat-treatment temperature, we could suggest that the temperature of formation of the sp^2 carbon substance in the meteorite studied on its way to Earth was in the range of $1500\text{--}2000^\circ\text{C}$.

It should be noted, that this form of sp^2 carbon along with other modifications (disordered graphite, sp^2 amorphous carbon) have been detected by the Raman method in the meteorites of various types, in the grains of a comet, and in stardust particles [89-91].

Lunar soil

Some fragments of lunar soil extracted by the Russian automatic station “Luna-24” from a deep part of the core in Mare Crisium (at a depth of 1.85 m) were investigated previously by the energy-dispersive X-ray analysis, SEM and back-scattered electron diffraction (BSE) [92, 93]. The results have shown that the crust of a large glass splinter contained the peaks of molybdenum, carbon, and oxygen. The BSE image has revealed that the crust consists of two parts: an internal molybdenum one and an external carbon-rich inclusion. However, the nature of carbonaceous substance detected in the paper [93] could not be elucidated by the methods applied in the study.

We have investigated by Raman micro-mapping about 20 fragments of $\sim 50 \times 50 \mu\text{m}$ size of the Lunar soil probes described in Ref. [92, 93]. Many spectra obtained contain only the features of the minerals present. However, in the spectra of some other locations, along with the bands corresponding to the minerals, the G, D and 2D bands were found typical of sp^2 carbon (Fig. 23). Detailed examination of this data set allowed us to conclude that the sp^2 carbonaceous substance in the probes belongs to three different modifications. A series of the spectra obtained (exemplified by Fig. 23a) along with the features assigned to minerals (at frequencies below 1000 cm^{-1}) exhibits the bands specific to turbostratic graphite with its irregular graphene layer arrangement. Another group of the spectra contains the bands similar to those of glassy carbons and shungites, the substances containing sp^2 nano-crystallites with some curved fragments (Fig. 23b). And the rest group of the spectra (exemplified by Fig. 23c) shows very broad features typical of disordered amorphous sp^2 carbon.

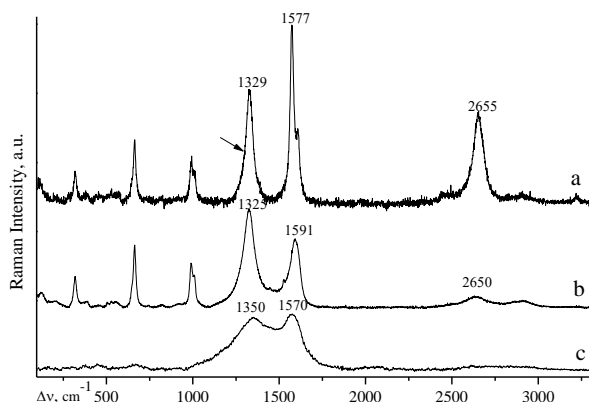


Fig. 23. Raman spectra of different micro-spots of carbon-enriched inclusions in Lunar soil.

Thus it is evident that carbon inclusions in the Lunar soil samples studied belong to three sp^2 carbon modifications. These are similar to terrestrial turbostratic graphite, glassy carbon and amorphous carbon [94].

Conclusion

Summing up the Raman results obtained, it can be concluded that carbonaceous components of the man-made advanced materials and those found in natural terrestrial and extra-terrestrial species (Lunar soil, meteoritic matter) contain similar sp^2 carbon modifications. This speaks for the singleness of Nature's laws (on Earth, Moon and in cosmic space).

Raman measurements

The Raman spectra were recorded using LabRAM-300 system (Horiba Scientific Inc.) equipped with a microscope (magnification $50\times$ and $100\times$) and TV camera. Excitation wavelength was 632.8 nm of a He-Ne laser. Spectral resolution 2 cm^{-1} . Special care was

taken to avoid laser induced heating which could lead to sample damage. Therefore the incident laser power used was in the limits $0.05\text{-}5 \text{ mW}$ depending on the sample nature. Band frequencies were calibrated against the Si line at 520 cm^{-1} and gaseous N_2 line at 2230 cm^{-1} . Micro-mapping was performed with spatial resolution $\sim 1 \mu\text{m}$.

Acknowledgements

The authors are greatly indebted to A.S. Kotosonov, V.A. Tyumentsev, A.G. Ryabenko, Yu.A. Morozov, and A.V. Mokhov for sample delivery and helpful discussions. The work was supported by Russian Scientific Foundation (grant #18-29-19181).

References

- Raman, Ch. V.; Krishnan, K. S.; *Nature*, **1928**, *121*, 501.
- Landsberg, G. S.; Mandel'stam, L. I.; *Journal of Russian Physico-Chemical Society*, **1928**, *60*, 335.
- Levashova, A. I.; Kravtsov, A. V.; Chemical Technology of Carbonaceous Materials (in Russian), TPU Publishers, Tomsk, Russia, **2008**, pp109.
- Saito, R.; Hofmann, M.; Dresselhaus, G.; Jorio, A.; Dresselhaus, M. S.; *Adv. Phys.*, **2011**, *60*, 413-550.
- Jorio, A.; *ISRN Nanotechnology*, **2012**, ID 234216.
- Dresselhaus, M. S.; Dresselhaus, G.; Jorio, A.; Sattler, K. D.; (Eds); *Handbook of Nanophysics*, **2011**, *4*, 7/1-7/19.
- Jorio, A.; Dresselhaus, M. S.; Saito, R.; Dresselhaus, G.; Raman Spectroscopy in Graphene Related Systems, Wiley, Germany, **2011**.
- Dresselhaus, M. S.; Jorio, A.; Souza Filho, A. G.; Saito, R.; *Phil. Trans. R. Soc. A*, **2010**, *368*, 5355.
- Dresselhaus, M. S.; Jorio, A.; Saito, R.; *Ann. Rev. Cond. Matt. Phys.*, **2010**, *1*, 89.
- Dresselhaus, M. S.; Jorio, A.; Hofmann, M.; Dresselhaus, G.; Saito, R.; *Nano Lett.*, **2010**, *10*, 751.
- Pimenta, M. A.; Dresselhaus, G.; Dresselhaus, M. S.; Cancado, L. G.; Jorio, A.; Saito, R.; *Phys. Chem. Chem. Phys.*, **2007**, *9*, 1276.
- Dresselhaus, M. S.; Dresselhaus, G.; Saito, R.; Jorio, A.; *Physical Reports*, **2005**, *409*, 47.
- (a) Robertson, J.; *Materials Science and Engineering R*, **2002**, *37*, 129.
(b) Robertson, J.; *Adv. Phys.*, **2011**, *60*, 87.
- Ferrari, A. C.; Robertson, J.; (a) *Phys. Rev. B*, **2001**, *64*, 075414;
(b) *Phys. Rev. B*, **2000**, *61*, 14095.
- Campos, J. L. E.; Miranda, H.; Rabelo, C.; Sandoz-Rosado, E.; Pandey, S.; Riikonen, J.; Cano-Marquez, A. G.; Jorio, A.; *J. Raman Spectr.*, **2018**, *49*, 54.
- Bokobza, L.; Bruneel, J.-L.; Couzi, M.; *J. Carbon Research*, **2015**, *1*, 77.
- Childres, I.; Jauregui, L. A.; Park, W.; Cao, H.; Chen, Y. P.; New Developments in Photon Materials Research, Jang, J.I. (Ed.); V. 1, Ch. 19, Nova Science Publishers, NY, **2013**, 403.
- Castiglioni, C.; Negri, F.; Tommasini, M.; Di Donato, E.; Zerbi, G.; *Top. Appl. Phys.*, **2006**, *100*, 381.
- Lauer, J. L.; Raman spectra of quasi-elemental carbon, in Handbook of Raman Spectroscopy, Lewis, I. R., Edwards, H. G. M. (Eds.), Ch. 22, pp. 863-917, Marcel Dekker Inc., N-Y, **2001**.
- Huono, P. V.; *Fresenius J. Anal. Chem.*, **1996**, *355*, 596.
- Ferrari, A. C.; Meyer, J. C.; Scardaci, V.; Casiraghi, C.; Lazzeri, M.; Mauri, F.; Piscanec, S.; Jiang, D.; Novoselov, K. S.; Roth, S.; Geim, A. K.; *Phys. Rev. Lett.*, **2006**, *97*, 187401.
- Ferrari, A. C.; *Solid State Commun.*, **2007**, *143*, 47.
- Tuinstra, F.; Koenig, J. L.; *J. Phys. Chem.*, **1970**, *53*, 1126.
- Bukalov, S. S.; Mikhailitsyn, L. A.; Zubavichus, Ya. V.; Leites, L. A.; Novikov, Yu. N.; *Ros. Khim. Zh. (Russian Chemistry Journal, in Russian)*, **2006**, *50*, 83.
- Cuesta, A.; Dhamelincourt, P.; Laureyns J.; Martinez-Alonso, A. J.; Tasco, J. M. D.; *J. Mater. Chem.*, **1998**, *8*, 2875.
- Vander Wal, R. L.; Tomasek, A. J.; Street, K.; Thompson, W. K.; Hull, D. R.; Patent NASA/TM-2003-212214.

27. Maslova, O. A.; Ammar, M. R.; Guimbretière, G.; Rouzaud, J. N.; Simon, P.; *Phys. Rev. B*, **2012**, *86*, 134205.
28. Marshall, C. P.; Marshall, O. A.; *Astrobiology*, **2013**, *13*, 920.
29. Okuda, H.; Young, R. J.; Wolverson, D.; Tanaka, F.; Yamamoto, G.; Okabe, T.; *Carbon*, **2018**, *130*, 178.
30. Vazquez-Santos, M. B.; Geissler, E.; Laszlo, K.; Rouzaud, J. N.; Martinez-Alonso, A.; Tascon, J. M. D.; *J. Phys. Chem. C*, **2012**, *116*, 257.
31. Zickler, G. A.; Smarsly, B.; Gierlinger, N.; Peterlik, H.; Paris, O.; *Carbon*, **2006**, *44*, 3239.
32. Tai, F. C.; Lee, S. C.; Wei, C. H.; Tyan, S. L.; *Mater. Trans.*, **2006**, *47*, 1847.
33. Carbon Materials for Advanced Technologies; Burchell, T. D (Ed.), Pergamon, Amsterdam, **1999**, pp. 535.
34. Yamada, S.; Sato, H.; *Nature*, **1962**, *193*, 261.
35. Franklin, R. E.; *Acta Cryst.*, **1951**, *4*, 253-261.
36. Jenkins, G. M.; Kawamura, K.; Ban, L.; *Proc. Roy. Soc. A*, **1972**, *327*, 501.
37. Pesin, L. A.; Baitinger, E. M.; *Carbon*, **2002**, *40*, 295.
38. Harris, P. J. F.; (a) *Phylos. Mag.*, **2004**, *84*, 3159.
(b) Harris, P. J. F.; *J. Mater. Sci.*, **2013**, *48*, 565.
39. Harris, P. J. F.; *Critical Reviews in Solid State and Materials Sciences*, **2005**, *30*, 235.
40. Solopova, N. A.; Dubrovinskaja, N.; Dubrovinsky, L.; *Appl. Phys. Lett.*, **2013**, *102*, 121909.
41. Petersen, T. C.; Snook, I. K.; Yarovsky, I.; McCulloch, D. G.; O'Malley, B.; *J. Phys. Chem. C*, **2007**, *111*, 802.
42. Powles, R. C.; Marks, N. A.; Lau, D. W. M.; *Phys. Rev. B*, **2009**, *79*, 075430.
43. Kotosonov, A. S.; *JETP Lett.*, **1986**, *43*, 30-32; *Sov. Phys. Sol. State*, **1991**, *33*, 2616.
44. Bukalov, S. S.; Zubavichus, Ya. V.; Leites, L. A.; Sorokin, A. I.; Kotosonov, A. S.; *Nanosystems: Physics, Chemistry, Mathematics*, **2014**, *1*, 1.
45. Baranov, A. V.; Bekhterev, A. N.; Bobovich, Ya. S.; Petrov, V. I.; *Optics and Spectroscopy*, **1987**, *62*, 1036.
46. Wilhelm, H.; Lelaurnin, M.; McRae, E.; Humbert, B.; *J. Appl. Phys.*, **1998**, *84*, 6552.
47. Tan, P. H.; Dimovsky, S.; Gogotsi, Yu.; *Phil. Trans. R. Soc. Lond. A*, **2004**, *362*, 2289.
48. Roy, D.; Chhowalla, M.; Wang, H.; *Chem. Phys. Lett.*, **2003**, *373*, 52.
49. Chand, S.; *J. Mater. Sci.*, **2000**, *35*, 1303.
50. Rahaman, M. S. A.; Ismail, A. F.; Mustafa, A.; *Mater. Sci. Eng.*, **2007**, *448*, 275.
51. Walsh, P. J.; *ASM Handbook*, **2001**, *21*, 35.
52. Naito, K.; Yang, J.M.; Xu, Y.; Kagawa, Y.; *Carbon*, **2010**, *48*, 1849.
53. Fitzer, E.; Mullier, D. J.; *Carbon*, **1975**, *13*, 63.
54. Sauder, C.; Lamon, J.; Pailler, R.; *Composites Sci. Technol.*, **2002**, *62*, 499.
55. (a) Tyumentsev, A. V.; Fazlitdinova, A. G.; *Techn. Phys.*, **2016**, *61*, 380.
(b) Tyumentsev, A. V.; Fazlitdinova, A. G.; *Techn. Phys.*, **2015**, *60*, 1705.
56. Fazlitdinova, A. G.; Tyumentsev, V. A.; Podkopaev, S. A.; Shveikin, G. P.; *J. Mater. Sci.*, **2010**, *45*, 3998.
57. Lee, S.; Kim, J.; Ku, B.C.; Kim, J.; Joh, H.-I.; *Adv. Chem. Eng. Sci.*, **2012**, *2*, 275.
58. He, D. X.; Wang, C. G.; Bai, Y. J.; Lun, N.; Zhu, B.; Wang, Y. X.; *J. Mater. Sci.*, **2007**, *42*, 7402.
59. Wang, B.; Xiao, Sh.; Cao, W.; Shi, X.; Xu, L.; *J. Appl. Polym. Sci.*, **2012**, *124*, 3413.
60. Tuinstra, F.; Koenig, J. L.; *J. Compos. Mater.*, **1970**, *4*, 492.
61. Zhou, Zh.; Wang X.; Faraji, Sh.; Bradford, P. D.; Li, Q.; Zhu, Y.; *Carbon*, **2014**, *75*, 307.
62. Li, D.; Wang, H.; Wang, X.; *J. Mater. Sci.*, **2007**, *42*, 4642.
63. (a) Huang, Y.; Young, R. J.; *Carbon*, **1995**, *33*, 97.
(b) Young, R. J.; *J. Text. Inst.*, **1995**, *86*, 360.
64. Montes-Moran, M. A.; Young, R. J.; *Carbon*, **2002**, *40*, 845.
65. (a) Fauteux, C.; Pegna, J.; *Appl. Phys. A*, **2004**, *78*, 883.
(b) Fauteux, C.; Longtin, R.; Pegna, J.; Boman, M.; *J. Appl. Phys.*, **2004**, *95*, 2737.
66. Lee, S.; Kim, J.; Ku, B.C.; Kim, J.; Joh, H.I.; *Adv. Chem. Eng. Sci.*, **2012**, *2*, 275.
67. Roh, J.-S.; *Carbon Lett.*, **2008**, *9*, 127.
68. Bukalov, S. S.; Leites, L. A.; Goloveshkin, A. S.; Dunaev, A. V.; Tyumentsev, V. A.; Fazlitdinova, A. G.; *Russ. Chem. Bull.*, **2018**, 1002.
69. Morita, K.; Murata, Y.; Ishitani, A.; Murayama, K.; Ono, T.; Nakajima, A.; *Pure Appl. Chem.*, **1986**, *58*, 455.
70. Misra, P.; Casimir, D.; Garcia-Sanchez, R.; *Proceedings of the Annual International Conference on Optoelectronics, Photonics & Applied Physics*, **2013**, *1*, 52.
71. Anoshkin, I. V.; Nefedova, I. I.; Lioubtchenko, D. V.; Nefedov, I. S.; Raicsaenen, A. V.; *Carbon*, **2017**, *116*, 547.
72. Ryabenko, A. G.; Kiryukhin, D. P.; Kichigina, G. A.; Zhigalina, O. M.; Sul'yanov, S. N.; Nikolaev, E. N.; Larichev, M. N.; Bukalov, S. S.; Krasnovskii, A. N.; *High Energy Chemistry*, **2015**, *49*, 53.
73. Corio, P.; Santos, P. S.; Pimenta, M. A.; Dresselhaus, M. S.; *Chem. Phys. Lett.*, **2002**, *360*, 557.
74. Calizo, I.; Balandin, A. A.; Bao, W.; Miao, F.; Lau, C. N.; *Nano Lett.*, **2007**, *7*, 2645.
75. Filippov, M. M.; *Proceedings of the Karelian Research Centre of RAS (in Russian)*, **2014**, 115.
76. a) Krasnovyud, S. V.; Konchits, A. A.; Shanina, B. D.; Valakh, M. Ya.; Yanchuk, I. B.; Yukhymchuk, V. O.; Yefanov, A. V.; Skoryk, M. A.; *Nanoscale Research Letters*, **2015**, *10*, 1.
(b) Konchits, A. A.; Shanina, B. D.; Valakh, M. Ya.; Yanchuk, I. B.; Yukhymchuk, V. O.; Yefanov, A. V.; Krasnovyud, S. V.; Skoryk, M. A.; *Func. Mater.*, **2014**, *21*, 260.
77. Kovalevsky, V. V.; (a) *Russ. J. Inorg. Chem.*, **1994**, *39*, 31;
(b) *Proceedings of the Russian Mineralogical Society*, **2011**, *CXXXVIII*, 97.
78. Kholodkevich, S. V.; Berezkin, V. I.; Davydov, V. Yu.; *Phys. Solid State*, **1999**, *41*, 1291.
79. Sheka, E. F.; Rozhkova, N. N.; *Proceedings of the Karelian Research Centre of RAS (in Russian)*, **2015**, 1.
80. Morozov, Yu. A.; Bukalov, S. S.; Leites L. A.; *Geophysical Investigations*, **2016**, *17*, 5.
81. Nazarov, M. A.; *Meteoritic Bulletin*, **2013**, 101, MAPS 47.
82. Anfilogov, V. N.; Belogub, E. V.; Blinov, I. A.; Eremyashev, V. E.; Kabanova, L. Ya.; Lebedeva, S. M.; Lonshchakova, G. F.; Khvorov, P. V.; *Lithosphera*, **2013**; No.3 (in Russian).
83. Voropaev, S. A.; Sevastyanov, V. S.; Eliseev, A. A.; Petukhov, D. I.; *Geochemistry*, **2013**, 654.
84. Bukalov, S. S.; Aysin, R. R.; Leites, L. A.; Eremyashev, V. E.; (a) *Rus. Chem. Bull.*, **2013**, *62*, 1129.
(b) *Carbon*, **2013**, *64*, 537.
85. Zhang, S. L.; Raman Spectroscopy and its Application in Nanostructures, Wiley, **2012**, p. 326.
86. Linares, R.; Doering, P.; *Diam. Relat. Mater.*, **1999**, *8*, 909.
87. Chrenko, R. M.; *J. Appl. Phys.*, **1988**, *63*, 5873.
88. Karczemska, A. T.; *J. Achievements Mater. Manuf. Eng.*, **2010**, *43*, 94.
89. (a) Wopenka, B.; Xu, Y. C.; Zinner, E.; Amari, S.; *Geochim. Cosmochim. Acta*, **2013**, *106*, 463.
(b) Wopenka, B.; *Meteor. Planet. Sci.*, **2012**, *47*, 565.
90. Ammar, M. R.; Charon, E.; Rouzaud, J.-N.; Aleon, J.; Guimbretiere, G.; Simon, P.; *Spectr. Lett.*, **2011**, *44*, 535.
91. Le Guillou, C.; Rouzaud, J. N.; Remusat, L.; Jambon, A.; Bourrot-Denise, M.; *Geochim. Cosmochim. Acta*, **2010**, *74*, 4167.
92. Mokhov, A. V.; Kartashov, P. M.; Bogatikov, O. A.; Magazina, L. O.; Ashikhmina, N. A.; Kopolulina, E. V.; *Doklady Earth Sciences*, **2007**, *415*, 926.
93. Mokhov, A. V.; Gornostaeva, T. A.; Kartashov, P. M.; Bogatikov, O. A.; Sakharov, O. A.; Trubkin, N. V.; *Doklady Earth Sciences*, **2016**, *471*, 1154.
94. Mokhov, A. V.; Bukalov, S. S.; Gornostaeva, T. A.; Leites, L. A.; Aysin, R. R.; Kartashov, P. M.; Bogatikov, O. A.; *Doklady Earth Sciences*, **2019**.